Nanoscale

PAPER

View Article Online
View Journal | View Issue

Cite this: *Nanoscale*, 2021, **13**, 4262

Microsphere-coupled light emission control of van der Waals heterostructures†

Hyunseung Lee,[a] Van Tu Nguyen,[a,b] Ji-Yong Park[a] and Jieun Lee[*a,c]

Received 9th September 2020,
Accepted 23rd January 2021

DOI: 10.1039/d0nr06510b

rsc.li/nanoscale

Two-dimensional transition metal dichalcogenides (TMDCs) integrated into photonic structures provide an intriguing playground for the development of novel optoelectronic devices with improved performance. Here, we show the enhanced light emission from TMDC based van der Waals heterostructures through coupling with microsphere cavities. We observe cavity-induced emission enhancement of TMDC materials which varies by an order of magnitude, depending on the size of the microsphere and thickness of the supporting oxide substrate. Furthermore, we demonstrate microsphere cavity-enhanced electroluminescence of a van der Waals light emitting transistor, showing the potential of 2D material based hybrid optoelectronic structures.

Introduction

Semiconductor transition metal dichalcogenides (TMDCs) have recently emerged as promising candidates for photonic and optoelectronic applications due to their unique optical and electronic properties.[1,2] When thinned down to monolayers, these two-dimensional (2D) materials exhibit direct bandgaps ranging from visible to near-infrared with strong excitonic emission in contrast to their bulk counterparts.[3,4] The optical characteristics of monolayer TMDCs are widely tunable by varying the thickness, doping, external fields and surrounding optical environment,[5–8] making these materials excellent candidates for the development of optoelectronic devices such as light emitters, photodetectors, and optical modulators.[9–12] However, the overall quantum yield of monolayer TMDCs is reported to be low because of considerable nonradiative recombination processes.[13] It has been suggested that the quantum yield of TMDCs can be controlled by changing their optical environments, *e.g.*, by integrating these materials into optical microcavities or modulating substrate materials and geometries.[12,14,15,40]

Integrating TMDCs into optical microcavities is reported to increase the photoluminescence (PL) emission of TMDCs through the enhancement of the local density of optical states due to the Purcell effect.[16] Recently, tailoring the PL emission of monolayer TMDCs by integrating into various types of optical cavities has been reported using Bragg reflectors, photonic crystal cavities and ring resonators.[12,14,15,17–20] Although these examples incorporate sophisticated cavity design and facilitate high quality (Q) factors of cavities, complicated processes during fabrication hinder the practical application of cavity-coupling schemes. Using microspheres, on the other hand, can bypass these complex fabrication processes, allowing simple and effective ways to couple TMDC monolayers to high Q microcavities. By bringing microspheres to the proximity of TMDC monolayers, it is possible to guide the emitted PL from the TMDCs to the surface of the cavity through the whispering gallery mode (WGM), thus enhancing light extraction.[21–23] Such coupling between the microsphere and TMDC monolayer has been demonstrated for monolayer MoS_2 directly grown on the curved surface of microspheres.[24] However, the deterministic coupling of microspheres to 2D material heterostructures has not been reported yet, which is essential for the development of a variety of 2D van der Waals material based photonic architectures.

In this work, we show the direct coupling of microsphere cavities on an arbitrary planar monolayer TMDC and demonstrate cavity-induced emission control. The observed emission intensity varies drastically with the cavity diameter. Also, by increasing the supporting oxide thickness, we observe high Q cavity modes of microspheres coupled to the TMDCs. Furthermore, through the direct coupling of microsphere cavities to the TMDC, graphene, and hexagonal boron nitride van der Waals heterostructures, we demonstrate microsphere-enhanced light extraction from electrically driven 2D light-emitting transistors. Our results show the potential of the designated structures of microsphere cavity coupled 2D

[a]*Department of Physics and Department of Energy Systems Research, Ajou University, Suwon 16499, Korea*
[b]*Institute of Materials Science, Vietnam Academy of Science and Technology, Hanoi, 100000, Vietnam*
[c]*Institute of Applied Physics and Department of Physics and Astronomy, Seoul National University, Seoul 08826, Korea. E-mail: lee.jieun@snu.ac.kr*
†Electronic supplementary information (ESI) available. See DOI: 10.1039/d0nr06510b

materials which will be useful for practical photonic and optoelectronic applications.

Results and discussion

Fig. 1a shows the schematics of the cavity-coupled TMDC fabricated on a planar silicon dioxide (SiO_2) substrate. The TMDCs used in our work are WSe_2 and MoS_2 and monolayer flakes are prepared by mechanical exfoliation of bulk materials or chemical vapor deposition (CVD) synthesis method. The monolayer thickness of the TMDC is confirmed by optical contrast in microscope images and photoluminescence spectra (ESI Fig. S1†). These monolayer flakes are integrated with microspheres (diameter = 2, 5 and 7 μm) using the following method. The microspheres dispersed in water are dropcast on polydimethylsiloxane (PDMS) and dried for a few minutes. Then the microspheres on PDMS are transferred onto monolayer TMDC flakes on SiO_2 using a micrometer manipulator while observing under an optical microscope. During the transfer, we chose microspheres that are sparsely distributed on PDMS to obtain spatially isolated cavity systems. The final optical image of the integrated microcavity on a monolayer TMDC is shown in Fig. 1b. Our fabrication scheme is designed to deterministically couple a microsphere to a given monolayer TMDC. With this method, we could fabricate about 7 cavity-coupled systems out of 10 attempts. Such a high success rate is due to the soft adhesion of PDMS that can easily release the microspheres on the targeted areas.

Using the finite-difference time-domain (FDTD) calculation packages in Lumerical, we simulated the formation of the cavity mode of microspheres, which is shown in Fig. 1c. In the simulated mode profile, the WGM of the cavity is clearly shown on the edge of the microsphere. The enhancement of the emission efficiency by the microsphere cavity is examined by calculating the Q factor as a function of the spherical diameter. In Fig. 1d, the calculated Q is found to increase with the sphere size, suggesting a higher light extraction rate of TMDC coupled to a larger microsphere.[25] Although the calculated Q values are smaller than that obtained for microspheres in air,[26] we obtained a sizable Q of about 265 using a 7 μm diameter sphere that was on top of the SiO_2/Si layer. For microsphere diameters smaller than 3 μm, the cavity mode could not be formed due to the weak WGM confinement.

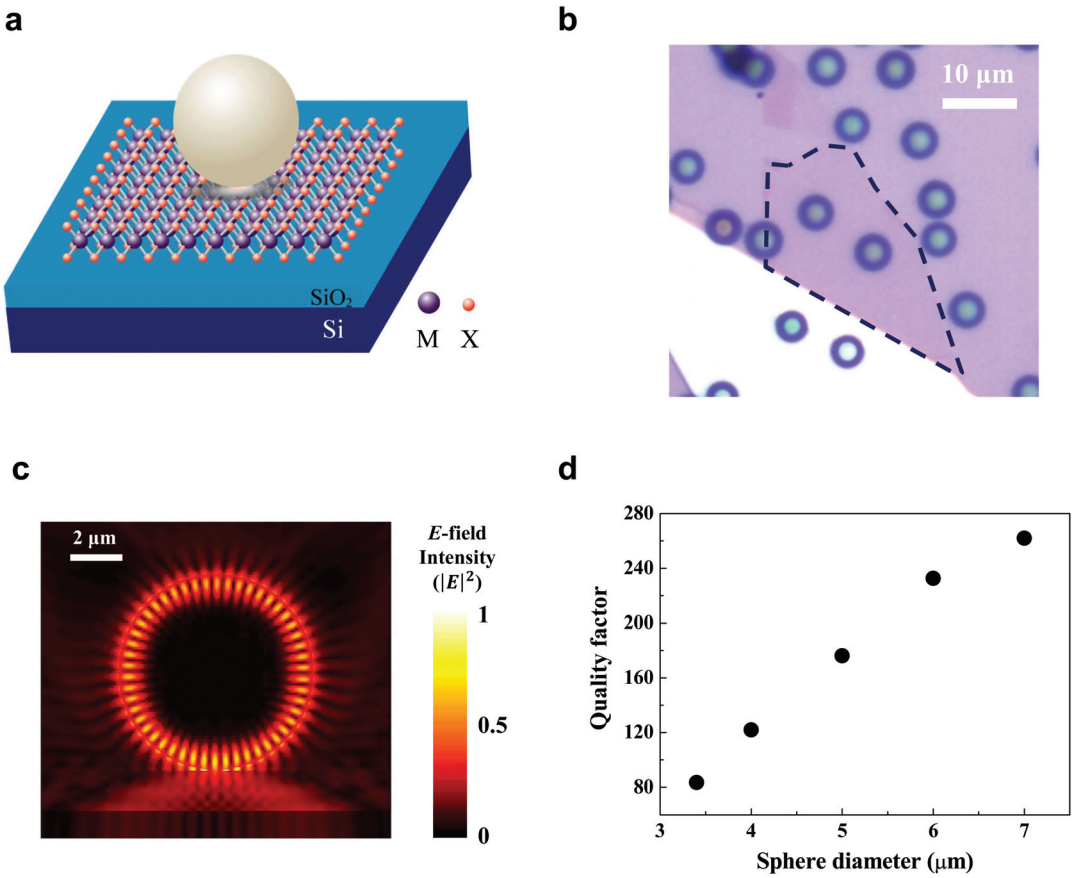

Fig. 1 (a) Schematic diagram of TMDC coupled to a microsphere on SiO_2/Si substrate. M and X refer to transition metal and chalcogen atom, respectively. (b) Optical microscope image of monolayer WSe_2 coupled to microspheres. (c) Finite-difference time-domain (FDTD) simulation of the whispering gallery mode of a microsphere (sphere diameter = 7 μm). Leakage mode into the substrate is observed due to the presence of an oxide layer. (d) Calculated Q factor as a function of the sphere diameter.

On the fabricated TMDC–microsphere coupled system, we performed photoluminescence (PL) measurement to investigate the cavity-induced emission enhancement. For the measurement, a continuous-wave laser (λ = 632.8 nm) is focused onto the sample with an objective lens (NA = 0.6) in normal incidence. The emitted light is collected using the same objective and analyzed with a spectrometer equipped with a charge-coupled device. In the measurement, we first obtained the PL spectrum of bare WSe_2 without a microsphere while focusing the laser spot on the WSe_2 layer. Then we moved the piezostage of the sample to measure the PL of WSe_2 coupled to a sphere. We observed up to 10 times enhancement of the PL intensity for WSe_2 coupled to a microsphere with the diameter of 7 μm as shown in Fig. 2a. We note that a micron thick oxide substrate was used. The enhancement rate increases as the sphere size increases from the comparison of the PL intensity normalized by the peak value of the bare WSe_2. Such emission enhancement of cavity-coupled WSe_2 was found locally only on the cavity-integrated area as verified from the spatially scanned 2D PL mapping (inset of Fig. 2a). Similar PL enhancement and the dependence on the microsphere size were observed for monolayer MoS_2 coupled with microspheres (ESI Fig. S2†).

In addition to the PL intensity enhancement, we also observed the red-shift of the emission energy of monolayer TMDC as a result of the cavity coupling. To verify the origin of the red-shifting emission spectrum, we performed temperature dependent measurement[41] and found that the observed red-shift increases at lower temperatures (ESI Fig. S3†). Such temperature dependence suggests that the asymmetry in the PL emission spectrum is associated with the exciton–phonon coupling which has also been observed in ring-resonator-coupled WSe_2[27] and nanocavity-integrated self-assembled quantum dot.[28] Although the PL reabsorption could also be in effect because of the overlap of the absorption line and the emission energy,[29] our observation of the systematic cavity-induced red-shift of the exciton energy as a function of temperature directly shows the evidence of the modulated exciton–phonon coupling in our system through the cavity integration.

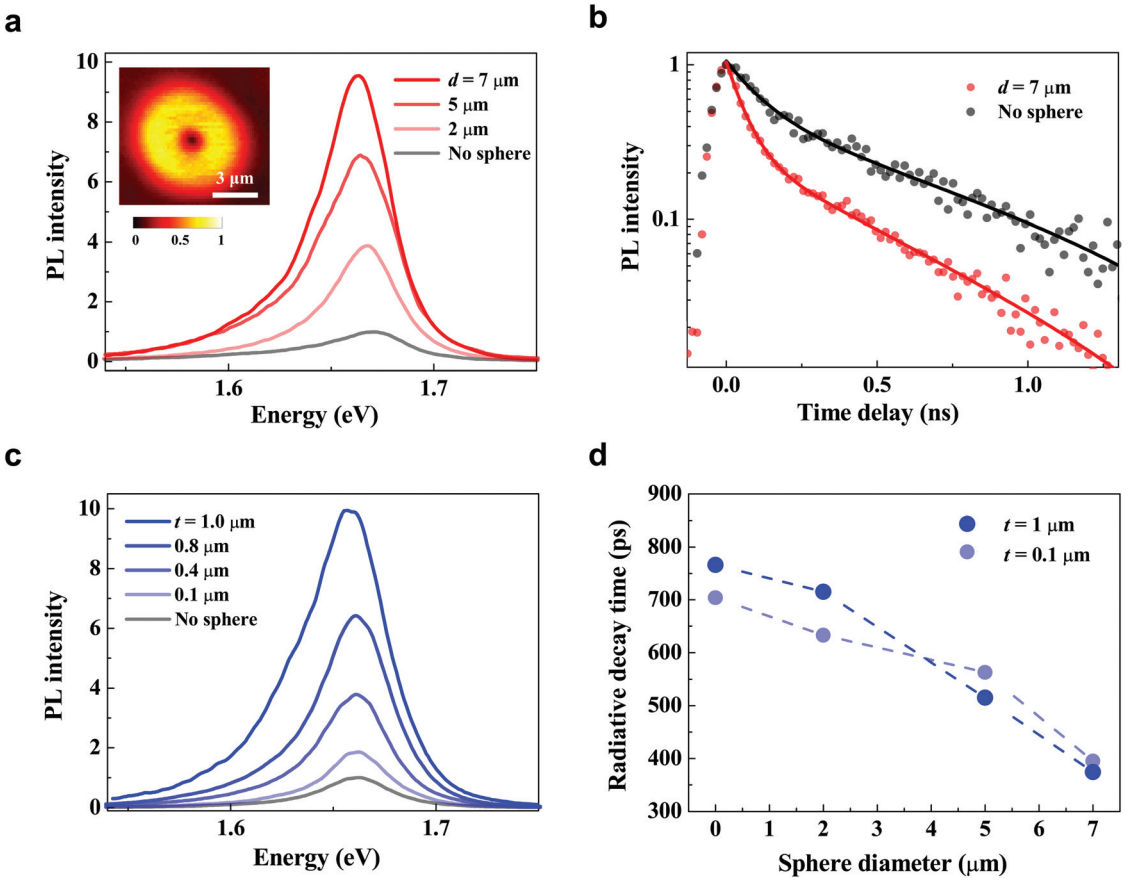

Fig. 2 (a) PL spectra of WSe_2 coupled to microspheres with varying diameters (d) on a micrometer thick oxide substrate. Each spectrum is normalized by the peak intensity of the PL measured on uncoupled WSe_2. Inset: Spatially scanned PL image of WSe_2 coupled to a 7 μm diameter sphere. (b) Time-resolved PL of WSe_2 coupled to a 7 μm diameter sphere (red dots) and WSe_2 without a microsphere (grey dots). Fit lines using biexponential decay functions are also shown. (c) PL spectra of WSe_2 coupled to a 7 μm diameter sphere with varying oxide thicknesses (t). Each PL spectrum is normalized by the peak intensity of the PL measured on uncoupled WSe_2 on the same substrate. The PL spectrum of uncoupled WSe_2 on 0.1 μm thick oxide is shown as a reference. (d) Radiative decay times of WSe_2 as a function of the sphere diameter for two different oxide thicknesses, t = 0.1 μm and 1 μm.

The emission efficiency enhancement due to the cavity mode is further studied by the direct measurement of the PL exciton lifetime using time-resolved photoluminescence (TRPL). In this experiment, a mode-locked Ti:Sapphire femtosecond laser pulse with the central wavelength tuned at 705 nm for the excitation of monolayer WSe_2 is focused onto the sample. The emitted PL is measured using the time-correlated single photon counting modules. Fig. 2b shows the temporal dynamics of the PL emission of monolayer WSe_2 coupled to a microsphere cavity of 7 μm diameter (red dots). A faster decay time due to the cavity coupling is observed with respect to the bare WSe_2 (grey dots).[30] By fitting the trace to a biexponential function, $I(t) = A\exp(-t/\tau_{Th}) + B\exp(-t/\tau_X)$, we extracted the parameters relevant to the decay dynamics. Here τ_{Th} and τ_X are the thermal dissipation time of hot carriers and the exciton recombination lifetime and A and B are the corresponding weight factors, respectively. Significant reductions of both τ_{Th} and τ_X were observed when monolayer WSe_2 is coupled to a microsphere cavity (details in the ESI Fig. S4†). By varying the microsphere size, the exciton recombination lifetime is modified accordingly as shown in Fig. 2d, demonstrating the Purcell enhancement of light extraction originating from the microsphere induced cavity coupling.

We have also observed that the PL intensity enhancement of cavity-coupled TMDC is largely dependent on the thickness of the oxide substrate. The systematic wet-etching of the substrate was employed to vary the oxide thickness, which ranges from 100 nm to 1 μm. The PL enhancement factor was then measured for monolayer WSe_2 coupled to individual microspheres on different substrates for the same microsphere size. In Fig. 2c, the measured PL enhancement rate is found to increase with increasing oxide thickness. Note that in each data, the PL spectrum of cavity-coupled WSe_2 is normalized by the peak PL intensity of bare WSe_2 on the same substrate. This suggests that the mechanism of light collection using microsphere cavity is sensitive to the optical environments and the substrate geometry. Since the TRPL measurement shows the negligible dependence of the recombination lifetime on the oxide thickness (Fig. 2d), we deduce that an additional geometrical factor other than the Purcell effect is playing a role. The geometrical factor can be understood as the enhanced collection efficiency of emitted light through the combination of the microsphere with the high NA objective lens. Such a lensing effect increases the light collection efficiency from the TMDC for a thicker oxide substrate because of an enhanced photonic jet mode,[31,32] which is a critical factor when developing optoelectronic devices using microspheres.

Using the micrometer-thick oxide substrate and integrating into a 7 μm diameter microsphere, we then directly observed the WGM of a cavity as shown in Fig. 3a. The CVD grown MoS_2 with the size of a few micrometers uniformly distributed on an oxide substrate was employed to fabricate TMDC-cavity coupled systems.[33] Several cavity modes with narrow linewidths are clearly observed.[34,35] Because of the flake size comparable to the contact area between the cavity and TMDC, the cavity modes are readily observed through the coupling of the emitted light into the microsphere. To better visualize the cavity modes, we then subtracted the spectrum in Fig. 3a by that measured on a nearby uncoupled MoS_2. The resulting spectrum is shown in Fig. 3b. The WGM peaks indicated by blue arrows agree well with the theoretical ones obtained from the FDTD simulation results. Also, the experimentally obtained cavity Q was about 259 reaching the theoretical limit, showing the high quality of the integrated optical structure.

Finally, we fabricated TMDC based light-emitting transistor and demonstrated the enhancement of the cavity-coupled electroluminescence (EL) to test the feasibility of integrating microsphere cavities with van der Waals heterostructure devices. In the structure, monolayer WSe_2 is encapsulated by two hexagonal boron nitrides as insulating layers and two few-

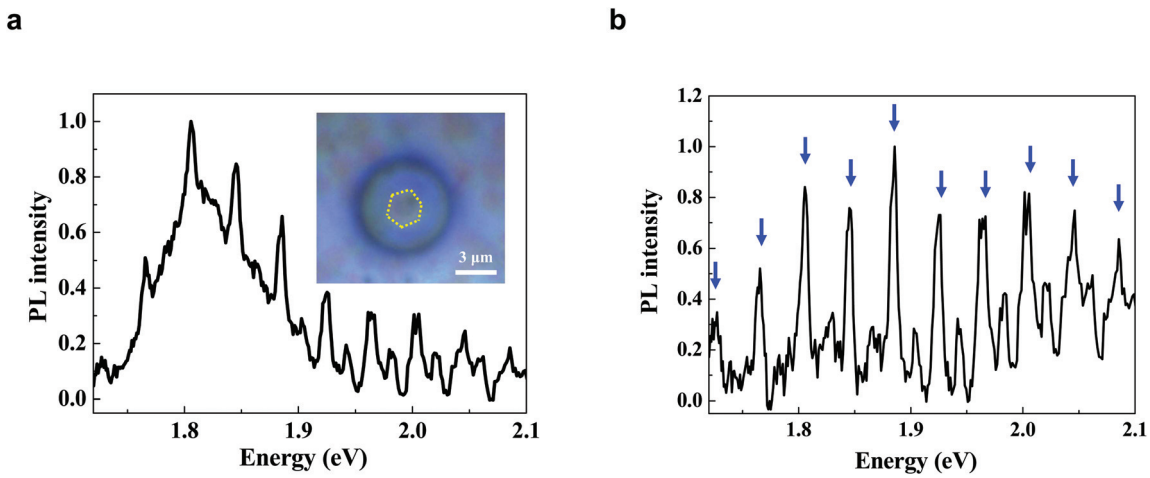

Fig. 3 (a) PL spectrum of monolayer MoS_2 coupled to a 7 μm diameter microsphere on a 1 μm thick oxide substrate. Inset: Optical microscope image of the CVD-grown MoS_2 with the integrated microsphere. The boundary of the MoS_2 coupled to the microsphere is indicated by yellow dashed lines. (b) PL spectrum of the cavity-coupled MoS_2 shown in (a) subtracted by that of the uncoupled MoS_2. The energies of the calculated WGMs are indicated by blue arrows.

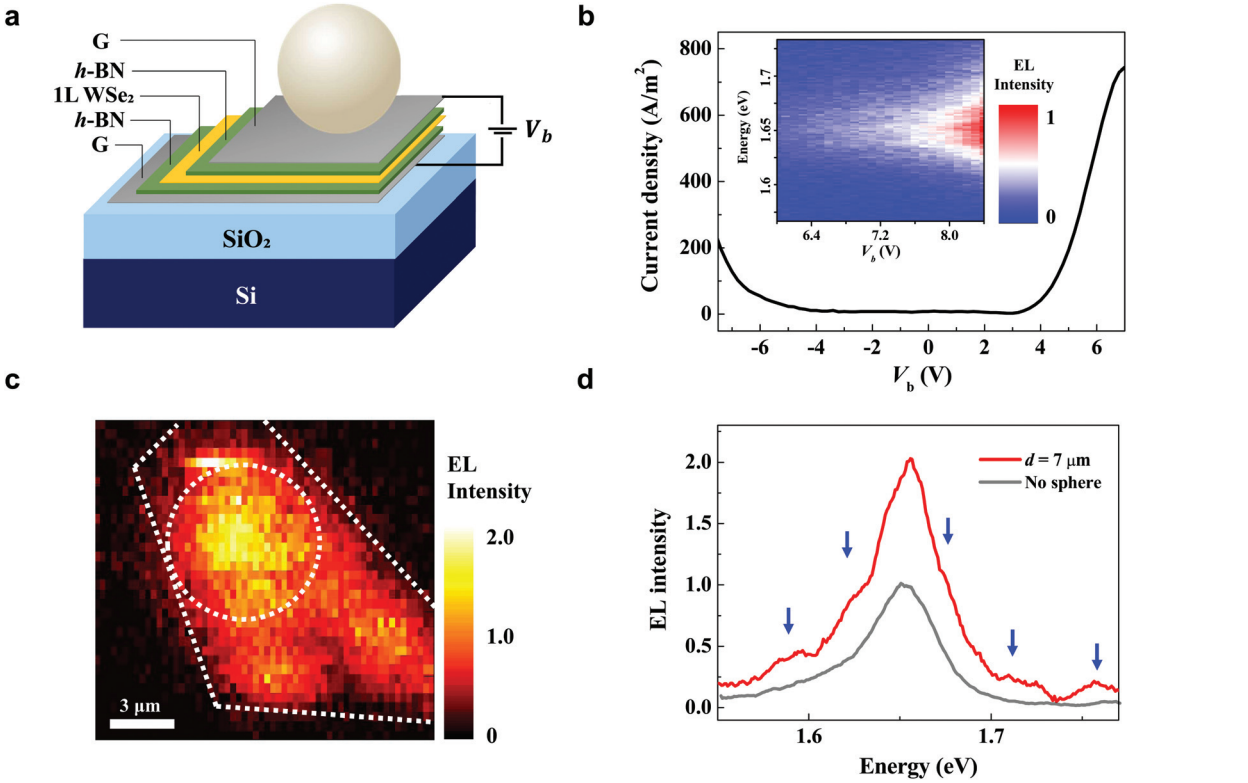

Fig. 4 (a) Schematics of the microsphere-coupled van der Waals heterostructure as an efficient light-emitting transistor. Monolayer (1L) WSe_2 is encapsulated between two few-layer h-BN to avoid the direct contact with top and bottom graphene (G). (b) Tunneling current density as a function of the bias voltage (V_b). Inset: The color map of the electroluminescence (EL) as a function of the bias voltage and energy. (c) Spatial scan image of the EL from the cavity-coupled WSe_2 light-emitting transistor. Boundaries of the monolayer WSe_2 and the coupled microsphere (d = 7 μm) are shown by white dashed lines. (d) EL spectra of the WSe_2 coupled to the microsphere (red solid line) and that without the microsphere (grey solid line). The calculated WGM energies are also shown (blue arrows).

layer graphene as top and bottom electrodes for the tunneling transistor operation[36] (Fig. 4a). The device structure utilizing graphene is designed for the pure electrical injection of the carriers in contrast to the previously reported TMDC heterostructures.[29,37] From electrical characterization, the onset of the tunneling current is observed at the bias voltage of about 4 V (Fig. 4b). By further increasing the bias, electrons and holes are injected into the monolayer WSe_2 and EL emission is induced as shown in the inset of Fig. 4b. The heterostructure is then integrated with a 7 μm microsphere using the method described above. On the final device, the cavity-induced modification of light extraction is examined by the 2D spatial mapping of the EL spectrum (Fig. 4c). Notably, we observed about a factor of 2 enhancement of EL intensity from WSe_2 coupled to the microsphere as shown in Fig. 4d. The signatures of WGMs are also observed, which are indicated by blue arrows. Such enhancement was absent in the EL map obtained without the cavity as in the ESI Fig. S5.† The observation manifests the microsphere-induced enhancement of light extraction from 2D heterostructure even without external optical pumping. By utilizing a microsphere, we could couple multiple cavity modes within the spectral range of the emitted light, which was possible due to the relatively short free spectral range of the microsphere employed in our work (~15 nm) compared to other cavities.[38]

Conclusion

In summary, we have shown the PL and EL emission control of monolayer TMDC through coupling to a microsphere cavity. The PL emission intensity enhancement of about 10 times is observed using a 7 μm diameter microsphere and a micrometer thick oxide substrate. High Q factors of the cavity WGM were observed through the controlled fabrication of a TMDC–microsphere coupled system. The observed emission modification is explained by the combination of the cavity Purcell enhancement and the microsphere ball lensing effect. In addition, we observed cavity induced enhanced EL emission from the TMDC based van der Waals heterostructure with the signature of the cavity modes, which can be further improved by optimizing the cavity design and fabrication methods.

We expect that integrating the microsphere cavity with 2D materials will be advantageous for the investigation of light–matter interactions in various regimes. For example, the coupling between the microsphere and 2D semiconductor does not

require polarization matching between the cavity mode and the emitting medium, which will allow the electron–photon interaction while maintaining the information on the electron's valley degree of freedom. The electrical pumping of the exciton emission demonstrated in our work will be potentially useful for the control of the carrier densities of cavity-coupled 2D materials which could lead to the observation of the exciton–polariton condensation. Furthermore, recent demonstration of the chip-based fabrication of microsphere[39] shows that the scalable integration of microspheres on silicon could be possible, providing a route towards the development of hybrid 2D photonic networks using microsphere cavities and on-chip photonic structures.

Conflicts of interest

There are no conflicts to declare.

Acknowledgements

The authors acknowledge the support from the National Research Foundation (NRF) of Korea (Grants No. 2020R1A2C2011334) and the "Human Resources Program in Energy Technology" of the Korea Institute of Energy Technology Evaluation and Planning (KETEP), granted financial resource from the Ministry of Trade, Industry & Energy, Korea (No. 20184030202220).

References

1 Q. H. Wang, K. Kalantar-Zadeh, A. Kis, J. N. Coleman and M. S. Strano, *Nat. Nanotechnol.*, 2012, **7**, 699–712.
2 K. S. Novoselov, A. Mishchenko, A. Carvalho and A. H. Castro Neto, *Science*, 2016, **353**, 461.
3 K. F. Mak, C. Lee, J. Hone, J. Shan and T. F. Heinz, *Phys. Rev. Lett.*, 2010, **105**, 136805.
4 A. Splendiani, L. Sun, Y. Zhang, T. Li, J. Kim, C. Y. Chim, G. Galli and F. Wang, *Nano Lett.*, 2010, **10**, 1271–1275.
5 A. Chernikov, A. M. Van Der Zande, H. M. Hill, A. F. Rigosi, A. Velauthapillai, J. Hone and T. F. Heinz, *Phys. Rev. Lett.*, 2015, **115**, 126802.
6 J. S. Ross, S. Wu, H. Yu, N. J. Ghimire, A. M. Jones, G. Aivazian, J. Yan, D. G. Mandrus, D. Xiao, W. Yao and X. Xu, *Nat. Commun.*, 2013, **4**, 1474.
7 H. S. Lee, S. W. Min, Y. G. Chang, M. K. Park, T. Nam, H. Kim, J. H. Kim, S. Ryu and S. Im, *Nano Lett.*, 2012, **12**, 3695–3700.
8 Y. C. Chen, H. Yeh, C. J. Lee and W. H. Chang, *ACS Appl. Mater. Interfaces*, 2018, **10**, 16874–16880.
9 J. S. Ross, P. Klement, A. M. Jones, N. J. Ghimire, J. Yan, D. G. Mandrus, T. Taniguchi, K. Watanabe, K. Kitamura, W. Yao, D. H. Cobden and X. Xu, *Nat. Nanotechnol.*, 2014, **9**, 268–272.
10 J. Pu and T. Takenobu, *Adv. Mater.*, 2018, **30**, 1707627.
11 N. Huo and G. Konstantatos, *Adv. Mater.*, 2018, **30**, 1801164.
12 B. Li, S. Zu, J. Zhou, Q. Jiang, B. Du, H. Shan, Y. Luo, Z. Liu, X. Zhu and Z. Fang, *ACS Nano*, 2017, **11**, 9720–9727.
13 L. Yuan and L. Huang, *Nanoscale*, 2015, **7**, 7402–7408.
14 X. Liu and V. M. Menon, *IEEE J. Quantum Electron.*, 2015, **51**, 0600308.
15 S. Wu, S. Buckley, A. M. Jones, J. S. Ross, N. J. Ghimire, J. Yan, D. G. Mandrus, W. Yao, F. Hatami, J. Vučković, A. Majumdar and X. Xu, *2D Mater.*, 2014, **1**, 011001.
16 K. J. Vahala, *Nature*, 2003, **424**, 839–846.
17 X. Gan, Y. Gao, K. F. Mak, X. Yao, R. J. Shiue, A. Van Der Zande, M. E. Trusheim, F. Hatami, T. F. Heinz, J. Hone and D. Englund, *Appl. Phys. Lett.*, 2013, **103**, 181119.
18 M. Förg, L. Colombier, R. K. Patel, J. Lindlau, A. D. Mohite, H. Yamaguchi, M. M. Glazov, D. Hunger and A. Högele, *Nat. Commun.*, 2019, **10**, 3697.
19 R. Maiti, C. Patil, R. A. Hemnani, M. Miscuglio, R. Amin, Z. Ma, R. Chaudhary, A. T. C. Johnson, L. Bartels, R. Agarwal and V. J. Sorger, *Opt. Mater. Express*, 2019, **9**, 751.
20 C. Liu, J. Zheng, Y. Chen, T. Fryett and A. Majumdar, *Opt. Mater. Express*, 2019, **9**, 384.
21 A. Chiasera, Y. Dumeige, P. Féron, M. Ferrari, Y. Jestin, G. N. Conti, S. Pelli, S. Soria and G. C. Righini, *Laser Photonics Rev.*, 2010, **4**, 457–482.
22 T. J. A. Kippenberg, *Nonlinear Optics in Ultra-High-Q Whispering-Gallery Optical Microcavities*, PhD Thesis, California Institute of Technology, 2004.
23 L. Zhao, Q. Shang, Y. Gao, J. Shi, Z. Liu, J. Chen, Y. Mi, P. Yang, Z. Zhang, W. Du, M. Hong, Y. Liang, J. Xie, X. Hu, B. Peng, J. Leng, X. Liu, Y. Zhao, Y. Zhang and Q. Zhang, *ACS Nano*, 2018, **12**, 9390–9396.
24 Y. Mi, Z. Zhang, L. Zhao, S. Zhang, J. Chen, Q. Ji, J. Shi, X. Zhou, R. Wang, J. Shi, W. Du, Z. Wu, X. Qiu, Q. Zhang, Y. Zhang and X. Liu, *Small*, 2017, **13**, 1701694.
25 I. H. Agha, J. E. Sharping, M. A. Foster and A. L. Gaeta, *Appl. Phys. B: Lasers Opt.*, 2006, **83**, 303–309.
26 K. Wang, Z. Gu, S. Liu, W. Sun, N. Zhang, S. Xiao and Q. Song, *J. Phys. Chem. Lett.*, 2016, **7**, 2549–2555.
27 D. Rosser, T. Fryett, A. Ryou, A. Saxena and A. Majumdar, *npj 2D Mater. Appl.*, 2020, **4**, 20.
28 A. Arora, M. Koperski, K. Nogajewski, J. Marcus, C. Faugeras and M. Potemski, *Nanoscale*, 2015, **7**, 10421–10429.
29 R. Khelifa, P. Back, N. Flöry, S. Nashashibi, K. Malchow, T. Taniguchi, K. Watanabe, A. Jain and L. Novotny, *Nano Lett.*, 2020, **20**, 6155–6161.
30 S. Schwarz, S. Dufferwiel, P. M. Walker, F. Withers, A. A. P. Trichet, M. Sich, F. Li, E. A. Chekhovich, D. N. Borisenko, N. N. Kolesnikov, K. S. Novoselov, M. S. Skolnick, J. M. Smith, D. N. Krizhanovskii and A. I. Tartakovskii, *ACS Nano*, 2014, **14**, 7003–7008.
31 A. Heifetz, S.-C. Kong, A. Sahakian, A. Taflove and V. Backman, *J. Comput. Theor. Nanosci.*, 2009, **6**, 1979.
32 S. Lee, L. Li and Z. Wang, *J. Opt.*, 2014, **16**, 015704.

33 V. T. Nguyen, S. Ha, D.-I. Yeom, Y. H. Ahn, S. Lee and J.-Y. Park, *Curr. Appl. Phys.*, 2019, **19**, 1127.
34 G. C. Righini, Y. Dumeige, P. Féron, M. Ferrari, G. N. Conti, D. Ristic and S. Soria, *Riv. Nuovo Cimento*, 2011, **34**, 435–488.
35 L. Wang, X. Zhou, S. Yang, G. Huang and Y. Mei, *Photonics Res.*, 2019, **7**, 905.
36 F. Withers, O. Del Pozo-Zamudio, A. Mishchenko, A. P. Rooney, A. Gholinia, K. Watanabe, T. Taniguchi, S. J. Haigh, A. K. Geim, A. I. Tartakovskii and K. S. Novoselov, *Nat. Mater.*, 2015, **14**, 301–306.
37 P. Rivera, T. K. Fryett, Y. Chen, C.-H. Liu, E. Ray, F. Hatami, J. Yan, D. Mandrus, W. Yao, A. Majumdar and X. Xu, *2D Mater.*, 2020, **7**, 015027.
38 C.-H. Liu, G. Clark, T. Fryett, S. Wu, J. Zheng, F. Hatami, X. Xu and A. Majumdar, *Nano Lett.*, 2017, **17**, 200–205.
39 X. Jiang, M. Wang, M. Kuzyk, T. Oo, G.-L. Long and H. Wang, *Opt. Express*, 2015, **23**, 27260–27265.
40 J. Shi, J. Zhu, X. Wu, B. Zheng, J. Chen, X. Sui, S. Zhang, J. Shi, W. Du, Y. Zhong, Q. Wang, Q. Zhang, A. Pan and X. Liu, *Adv. Opt. Mater.*, 2020, **8**, 2001147.
41 Z. Jia, J. Shi, Q. Shang, W. Du, X. Shan, B. Ge, J. Li, X. Sui, Y. Zhong, Q. Wang, L. Bao, Q. Zhang and X. Liu, *ACS Appl. Mater. Interfaces*, 2019, **11**, 20566–20573.